Efficiency of Synaptic Transmission of Single-Photon Events from Rod Photoreceptor to Rod Bipolar Dendrite

Stan Schein*† and Kareem M. Ahmad*
*Department of Psychology and †Brain Research Institute, University of California, Los Angeles, California

ABSTRACT A rod transmits absorption of a single photon by what appears to be a small reduction in the small number of quanta of neurotransmitter (Q_{count}) that it releases within the integration period (~0.1 s) of a rod bipolar dendrite. Due to the quantal and stochastic nature of release, discrete distributions of Q_{count} for darkness versus one isomerization of rhodopsin (R*) overlap. We suggested that release must be regular to narrow these distributions, reduce overlap, reduce the rate of false positives, and increase transmission efficiency (the fraction of R* events that are identified as light). Unsurprisingly, higher quantal release rates (Q_{rates}) yield higher efficiencies. Focusing here on the effect of small changes in Q_{rate}, we find that a slightly higher Q_{rate} yields greatly reduced efficiency, due to a necessarily fixed quantal-count threshold. To stabilize efficiency in the face of drift in Q_{rate}, the dendrite needs to regulate the biochemical realization of its quantal-count threshold with respect to its Q_{count}. These considerations reveal the mathematical role of calcium-based negative feedback and suggest a helpful role for spontaneous R*. In addition, to stabilize efficiency in the face of drift in degree of regularity, efficiency should be ≈50%, similar to measurements.

INTRODUCTION

Extraordinarily sensitive sensory systems face two problems. First, the receptor cell must be able to transduce an extremely weak stimulus, a single photon in the case of a rod photoreceptor, nanometer bending in the case of a hair cell, and microvolts in the case of an electroreceptor. Second, and the subject of this and a prior article (1), the receptor cell must be able to transmit such a small electrical signal to its target neurons by a small change in the number of quanta (Q) of neurotransmitter that it releases in the integration period of a rod bipolar dendrite. The quantal and stochastic nature of neurotransmitter release, along with the small numbers of quanta involved, impose inescapable mathematical constraints on synaptic transmission from receptor cell to target neuron.

The synaptic terminals of these receptor cells have synaptic ribbons or ribbonlike structures that enable them to maintain a high rate of release of quanta of neurotransmitter (Q_{rate}) (2). The rate for a rod in the dark, $Q_{rate,dark}$, is thought to be ~100 Q s^{-1} (2–5), but may be lower (6). A rod bipolar dendrite accumulates quanta of neurotransmitter for ~0.1 s (7–10), considerably longer than the ~10-ms interval between quanta, so the dendrite may be regarded as a quantal counter. However, quantal release is a stochastic process, so the count of quanta in ~0.1 s in the dark ($Q_{count,dark}$) varies from epoch to epoch and would be distributed (e.g., *solid diamonds* in Fig. 1 *A*). The mean of the $Q_{count,dark}$ distribution is small, perhaps ~10 Q.

Upon absorption of one photon and isomerization of one rhodopsin molecule (from R to R*), the mammalian rod hyperpolarizes by only one millivolt (10–12) and is likely to reduce its Q_{rate} by only ~20% (1). The quantal count for one R* ($Q_{count,R*}$) would also be distributed (e.g., Fig. 1 *A*, *open squares*), and its mean is also small, perhaps ~8 Q. The reduction in Q_{count} would thus be very small, averaging just ~2 Q.

The quantal counter must have a threshold quantal count (Q_T) to discriminate R* events ($Q_{count} \leq Q_T$) from darkness ($Q_{count} > Q_T$). Such a nonlinearity was suggested by Baylor and colleagues (11), modeled by van Rossum and Smith (5), and located postsynaptically (13,14) in the bipolar dendrite, not presynaptically in the nearly linear rod terminal (15). Given overlapping $Q_{count,dark}$ and $Q_{count,R*}$ distributions, Q_T determines the probability of a false positive (when $Q_{count} \leq Q_T$ in the dark) and efficiency (the probability that $Q_{count} \leq Q_T$ after production of one R*). In our prior article, we described several ways to reduce overlap and thereby improve efficiency (1). Foremost, we argued that release cannot be random (Poisson) but must instead be regular (''clockwork'') to narrow the Q_{count} distributions. By studying the four $Q_{rates,dark}$, 50, 100, 200, and 400 Q s^{-1}, and various Q_T, we found that higher $Q_{rates,dark}$ yield higher efficiencies. However, by studying just those four $Q_{rates,dark}$, we missed a richer picture.

Here we change $Q_{rates,dark}$ in finer increments but with necessarily fixed Q_T. We show that efficiency is determined by a single parameter combining degree of regularity and $Q_{count,dark}$, so suitable adjustment of degree of regularity can achieve a high efficiency like 50% even for a very low $Q_{rate,dark}$ like 12 Q s^{-1}. However, a small increase in $Q_{rate,dark}$ greatly reduces efficiency. To stabilize efficiency in the face of potential drift in $Q_{rate,dark}$, the rod bipolar cell needs to

Submitted June 20, 2006, and accepted for publication August 4, 2006.

Address reprint requests to Stan Schein, University of California, Los Angeles, Dept. of Psychology, Franz Hall, Rm. 8522, Mailcode 951563, Los Angeles, CA 90095-1563. Tel.: 310-825-0505; Fax: 310-206-5895; E-mail: schein@ucla.edu.

0006-3495/06/11/3257/11 $2.00

doi: 10.1529/biophysj.106.091744

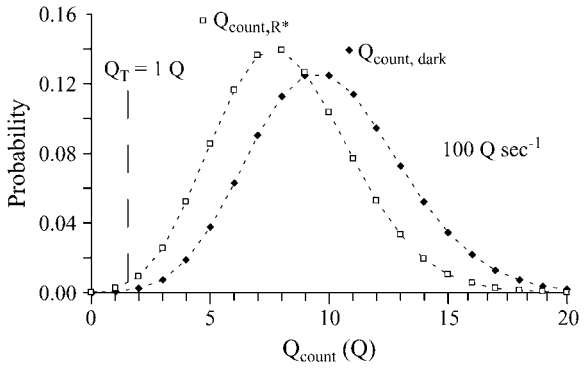

FIGURE 1 Quantal count distribution for random (Poisson) quantal release. Assuming a quantal release rate in the dark ($Q_{rate,dark}$) of 100 Q s^{-1} and a counting window of 0.1 s, the mean of the $Q_{count,dark}$ Poisson distribution (♦) is 10 Q. Assuming that the release rate after one isomerization of rhodopsin (from R to R*) falls by 20%, the mean of the Q_{count,R^*} Poisson distribution (□) is 8 Q. The standard deviation of each of these Poisson distributions is equal to the square root of the mean count. The probability that $Q_{count,dark}$ is ≤1 Q (*dashed vertical line*) is 1 in 2002 epochs of 0.1 s.

regulate the relationship between the biochemical realization of its Q_T and the biochemical realization of its Q_{count,R^*}, thus uncovering the mathematical role of negative feedback involving Ca^{2+} and suggesting a helpful role for spontaneous isomerization of rhodopsin. Efficiency could be stabilized in the face of drift in degree of regularity as well if median $Q_{count,R^*} \approx Q_T$ and efficiency = 50%, similar to what has been measured.

METHODS

Interval distributions and regular release

Regular quantal release is modeled as an Erlang renewal process (1). In this process, an Erlang Event is triggered at each rth underlying Poisson event. The higher the order r, the more regular the release process, the less variation in the interval between quanta, and the less variation in the number of quanta counted in a counting window. We suppose that release of a quantum, the Erlang Event, might follow accumulation of multiple (r) phosphorylations, the underlying Poisson events, of a synaptic protein like bassoon or piccolo (1,16).

In detail, the mean interarrival interval between rth-order Erlang Events is r times the mean interval between the underlying Poisson events. The standard deviation (SD) of the interval distribution also increases, but by $\sqrt{r}$, so the coefficient of variation (SD/mean) of the distribution falls, by $1/\sqrt{r}$. The interval distribution thus narrows by a factor N that equals the coefficient of variation of the interval distribution, $1/\sqrt{r}$.

A gamma process is a generalization of the Erlang process that allows noninteger order r. Regular release could also be modeled by a refractory period after each quantal release (17,18). We use Erlang and gamma processes because of their advantageous mathematical properties.

Number distributions and regular release

For a counting window of time T, for Poisson events occurring at rate α-events s^{-1}, the expected count of Poisson events is αT. For an rth-order ordinary Erlang renewal process, Erlang Events occur at rate α/r. The expected count of Erlang Events is related to a quantity $M = (\alpha/r)T$ (rate × time). In fact, the expected count of Erlang Events is slightly less than M (see Eq. A9 of Appendix A in Schein and Ahmad (1).) To see why, consider a very regular process with $M = 10$. The 10th Event would fall just before the end of the counting window T in ~50% of the trials and just after the end in the other trials, giving almost equal numbers of counts of 9 and 10 and an expected count close to 9.5. The probability distribution of the count narrows with increasing r, and the coefficient of variation falls by $\sim 1/\sqrt{r}$.

We explore different Q_{rates} in this article, but 100 Q s^{-1} is a good starting point: A mammalian rod has two ribbon synaptic units (19), and the patch or patches of mGluR6 receptors on a bipolar dendrite have access to quanta released by both ribbon synaptic units (4,19). The biological $Q_{rate,dark}$ for the active zone associated with each ribbon synaptic unit appears to be ~50 Q s^{-1}, a rate per ribbon suggested by ~400 Q s^{-1} for a salamander rod (3) with its ~7 ribbons (20). With its two-ribbon synaptic units, this rate also matches predictions of an overall $Q_{rate,dark}$ of 100 Q s^{-1} for mammalian rod (4,5).

We assume a counting window of 0.1 s (7,10). Because Q_{count} is the product of Q_{rate} and the counting window, doubling the counting window has virtually the same effect as doubling Q_{rate}, the main parameter that is studied in this article. Therefore, the effects of some other preferred counting window could be inferred from appropriately scaled Q_{rates}.

We assume a probability of false positives due to the combination of voltage and quantal noise of 1 in 16,000. With epochs of 0.1 s, the corresponding interval between these false positives would be 1600 s, 10 times the interval between spontaneous isomerizations of rhodopsin, 160 s (11). In that case, these false positives would not significantly increase the ''dark light'', suggested to be due to spontaneous isomerization of rhodopsin (21–23). This probability, 1/16,000, is not critical to any of the findings in this article. The precise value of some of the results would change by small amounts, but the qualitative findings would not (1).

We assume that, depending on Ca^{2+} current through the voltage dependent L-type Ca^{2+} channel in the rod terminal, Q_{rate} falls e-fold for a 5-mV hyperpolarization (3,24–26). Therefore, for a 1-mV hyperpolarization in response to one R*, Q_{rate} would fall to 81.9% of its value in the dark (1). For example, if Q_{rate} in the dark ($Q_{rate,dark}$) were 100 Q s^{-1}, it would fall to 81.9 Q s^{-1} for one R*. For a counting window of 0.1 s, mean Q_{count} would fall from ~10 Q to ~8 Q, a drop of ~2 Q for the 1-mV hyperpolarization.

The contribution of voltage noise and quantal noise to number distributions

Voltage noise, ±0.2 mV under physiological conditions, is equal to the SD of the membrane potential of the rod in the dark. This same amount of voltage noise also characterizes the membrane potential for one R* (11,12,27). This variation in rod voltage produces variation in presynaptic Q_{rate} and thus in postsynaptic Q_{count}. Above, we estimate a drop in Q_{count} of ~2 Q/mV, so SDs of ±0.2 mV in membrane potential distributions produce SDs of ~±0.4 Q in Q_{count} distributions (see Appendix B of Schein and Ahmad (1)).

For Poisson release at α-events s^{-1}, the mean interval between events would be $1/\alpha$ sec. The SD of the interval distribution would equal the mean interval, $1/\alpha$ sec. The mean Q_{count}, called λ, would equal the product of the rate (α) of Poisson events and the duration of the counting window (T), hence αT. Quantal noise, the SD of the Q_{count} distribution, would be $\sqrt{\alpha T}$ for Poisson release, generally greater than the SD contributed by voltage noise (1).

For an rth-order Erlang release process, with rate $A = \alpha/r$ Erlang Events s^{-1}, the mean interval $1/A$ would be r/α, and the SD of the interval distribution would be less than the mean interval r/α by the factor $1/\sqrt{r}$; that is, the SD would equal $\sqrt{r}/\alpha$ or $1/(A\sqrt{r})$. Of particular importance, the SD of the Q_{count} distribution would be less for Erlang release than for Poisson release by a factor of $\sim 1/\sqrt{r} = N$.

Both voltage noise and quantal noise contribute to the SD of the Q_{count}, as described in Appendix B of Schein and Ahmad (1). In brief, because voltage noise and quantal noise are independent, the SD of the Q_{count} distribution is approximately equal to the square root of the sum of the squares of the SD of the Q_{count} distribution due to voltage noise (with no quantal noise) and the SD of the Q_{count} distribution due to quantal noise (with no voltage noise). In

practice, we generate the actual joint probability distribution of Q_{count} to obtain the SD of the Q_{count} distribution (cf. Fig. 5 of Schein and Ahmad (1)).

RESULTS

Efficiency rises as Q_{rate} falls

The dark diamonds in the middle panel of Fig. 2 show the $Q_{count,dark}$ distribution for a quantal release rate in the dark ($Q_{rate,dark}$) of 100 Q s^{-1} and a counting window of 0.1 s. The mean Q_{count} is near 10 Q. With a quantal threshold (Q_T) set to 7 Q (Fig. 2, *dashed vertical line*), the distribution had to be narrowed considerably to achieve a probability that $Q_{count,dark} \leq$ 7 Q at 1 in 16,000 epochs (1600 s). The requisite narrowing (N) is 0.123, generated by a gamma order r of 66.5 Poisson events per Erlang Event.

Absorption of a photon and consequent production of one R* hyperpolarizes the rod, reduces Q_{rate} to 81.9 Q s^{-1}, and reduces mean $Q_{count,R*}$. The sum of the probabilities for values of $Q_{count,R*} \leq Q_T$, that is, for values of $Q_{count,R*}$ to the left of the dashed vertical line, is 34.2%. This value is the efficiency, the percent of R* events reported as an R* event.

Fig. 3 *A* shows the narrowing N that is needed to maintain the probability of false positives at 1/16,000 for $Q_T = 7$ Q and $Q_{rates,dark}$ that range from 93 to 140 Q s^{-1}. The narrowing N must rise as $Q_{rate,dark}$ rises; that is, less narrowing is needed for higher $Q_{rates,dark}$. Conversely, efficiency falls as $Q_{rate,dark}$ rises (Fig. 3 *B*). In light of our previous experience (1), with efficiency rising with increasing $Q_{rate,dark}$, this result was a surprise. We now explain this result.

A lower $Q_{rate,dark}$ like 96 Q s^{-1} produces a lower $Q_{count,dark}$ than does 100 Q s^{-1}. (Compare the *lower panel* with the *middle panel* in Fig. 2.) Because of its leftward shift, the $Q_{count,dark}$ distribution for 96 Q s^{-1} must be narrowed to place 1 in 16,000 of its counts at $\leq$7 Q. Indeed, N must be set to 0.074 for 96 Q s^{-1}, compared with 0.123 for 100 Q s^{-1}. Conversely, a higher $Q_{rate,dark}$ like 108 Q s^{-1} shifts the $Q_{count,dark}$ distribution rightward. (Compare Fig. 2, *upper* and *middle panels*.) That distribution need not be as narrow ($N = 0.199$) as that for 100 Q s^{-1} ($N = 0.123$).

As shown by the light squares in the middle panel of Fig. 2, an R* event reduces the $Q_{rate,dark}$ of 100 Q s^{-1} to a $Q_{rate,R*}$ that is 81.9% as much, 81.9 Q s^{-1}. As described above, 34.2% of the $Q_{count,R*}$ distribution is $\leq$7 Q, so the efficiency for reporting R* events is 34.2%.

As shown by the light squares in the lower panel of Fig. 2, an R* event reduces the lower $Q_{rate,dark}$ like 96 Q s^{-1} to a $Q_{rate,R*}$ that is 81.9% as great, 78.6 Q s^{-1}, <81.9 Q s^{-1}. Primarily for this reason, a higher percentage (64.2%) of the $Q_{count,R*}$ distribution is $\leq$7 Q.

If efficiency is >50%, as it is in the lower panel of Fig. 2, the median $Q_{count,R*}$ must be $\leq Q_T$, that is, $\leq$7 Q in this example. As a result, the narrowing of the $Q_{count.R*}$ distribution in the lower panel in Fig. 2 places even more of the counts at $\leq$7 Q and contributes secondarily to the high

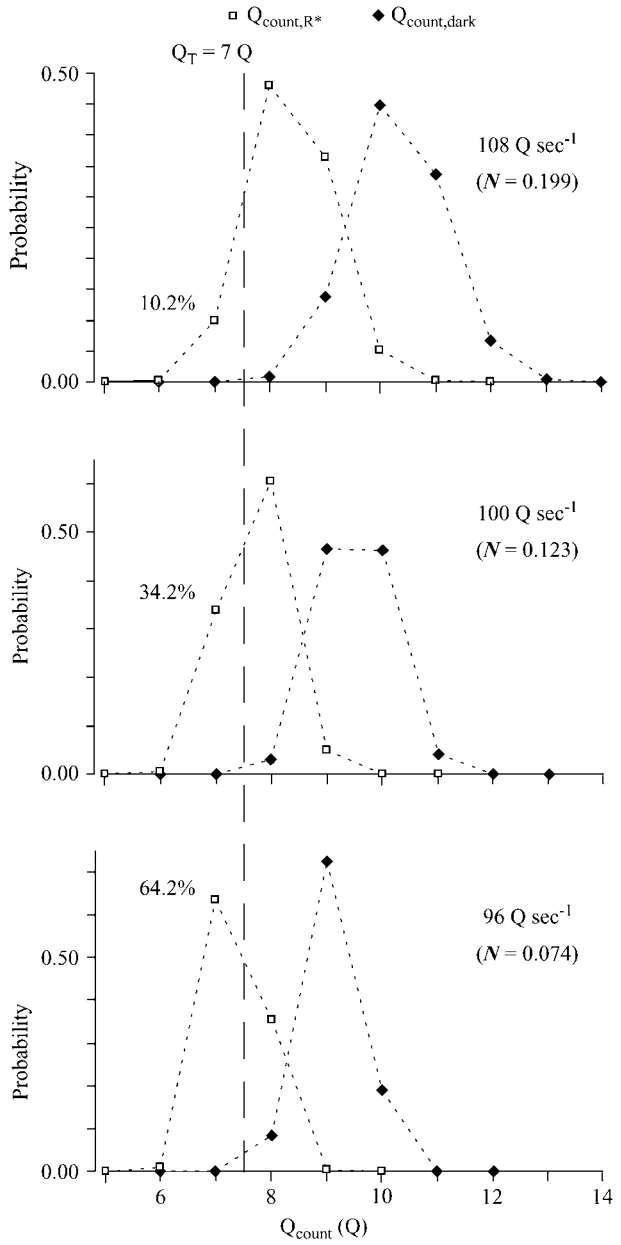

FIGURE 2 For a given quantal threshold Q_T, efficiency of transmission rises as $Q_{rate,dark}$ falls. The $Q_{rate,dark}$ generating the data in the upper panel is higher (108 Q s^{-1}) than the $Q_{rate,dark}$ generating the data in the middle panel (100 Q s^{-1}). The $Q_{rate,dark}$ generating the data in the lower panel is lower (96 Q s^{-1}) than that in the middle panel. A false positive occurs when the $Q_{count,dark}$ (♦) is $\leq Q_T$. Because a false positive occurs for $Q_{count,dark} \leq Q_T$ rather than $Q_{count,dark} < Q_T$, the Q_T of 7 Q is indicated by the dashed vertical line between 7 Q and 8 Q rather than at 7 Q. The probability of a false positive is the sum of the probabilities for values of $Q_{count,dark} \leq Q_T$, that is, to the left of the dashed vertical line. A true positive occurs when the $Q_{count,R*}$ (□) is $\leq Q_T$. Efficiency is the sum of the probabilities for values of $Q_{count,R*} \leq Q_T$, that is, to the left of the dashed vertical line. The narrowing N is set to give a probability of one false positive per 16,000 epochs (1600 s), the counting window is set to 0.1 s, and the decrement from $Q_{rate,dark}$ to $Q_{rate,R*}$ due to a 1-mV hyperpolarization is 18.1%, corresponding to an e-fold drop in Q_{rate} for a 5-mV hyperpolarization.

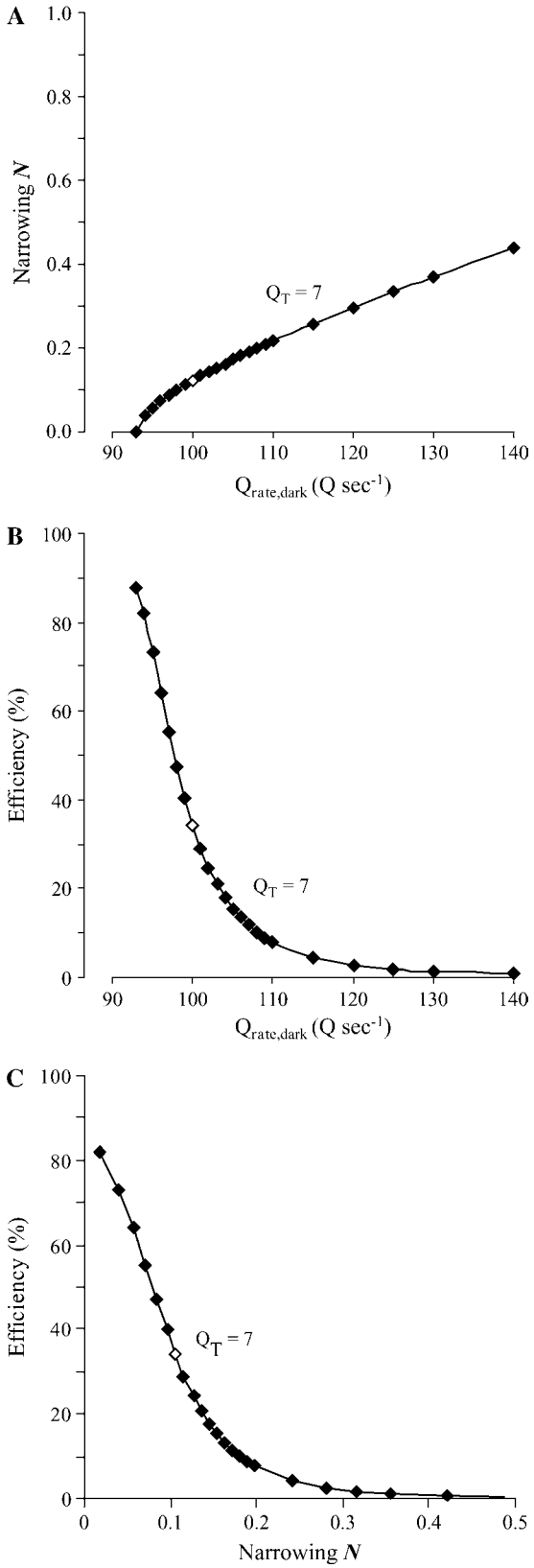

FIGURE 3 As $Q_{rate,dark}$ rises, less regularity is required, so narrowing N rises, and efficiency of transmission falls. (*A*) Narrowing N as a function of $Q_{rate,dark}$ for $Q_T = 7$ Q. (*B*) Efficiency as a function of $Q_{rate,dark}$ for $Q_T = 7$ Q. (*C*) Efficiency as a function of narrowing N for $Q_T = 7$ Q. These data rely on the same ''standard assumptions'' as in the legend of Fig. 2 for probability of false positives (1/16,000), duration of counting window (0.1 s), and decrement (18.1%). We sampled integer values of $Q_{rate,dark}$, starting with 93 Q s^{-1} and incrementing by 1, 2, and 5 Q s^{-1} for higher values of $Q_{rates,dark}$. Because $Q_{rate,dark}$ is not restricted to integers, points are connected by solid curves. The open symbol in each dataset marks $Q_{rate,dark}$ = 100 Q s^{-1}, $N = 0.123$, and efficiency = 34.2%.

efficiency. This latter phenomenon is illustrated in the lower panel of Fig. 4, which shows two Q_{count} distributions, one wider ($N = 1.0$), one narrower ($N = 0.5$), but both with the same mean Q_{count}. If the median $Q_{count.R*}$ is less than the threshold count (*dashed vertical line*), then the narrow distribution has a greater percentage of its counts to the left of the dashed line and has higher efficiency than the broad distribution.

As shown by the light squares in the higher panel of Fig. 2, an R* event reduces the higher $Q_{rate,dark}$ 108 Q s^{-1} to a $Q_{rate,R*}$ that is 81.9% as great, 88.5 Q s^{-1}, more than 81.9 Q s^{-1}. Primarily for this reason, a lower percentage (12.2%) of the $Q_{count,R*}$ is $\leq$7 Q.

If efficiency is $<$50%, as it is in this case, the median $Q_{count,R*}$ must be $>Q_T$, that is, $>$7 Q in this example. As a result, the narrowing of the $Q_{count.R*}$ distribution in the higher panel in Fig. 2 places even fewer of the counts at $\leq$7 Q and contributes secondarily to the low efficiency. This latter phenomenon is illustrated in the upper panel of Fig. 4. If the median $Q_{count.R*}$ is more than some threshold count (*dashed vertical line*), then the narrower distribution has a smaller percentage of its counts to the left of the threshold count and has a lower efficiency than the broad distribution.

For the data in Fig. 3, $Q_{rate,dark}$ ranges from 93 to 140 Q s^{-1}. For low rates, efficiency is very high (Fig. 3 *B*). For these low rates, the narrowing N must be practically 0 to achieve a probability of one false positive in 16,000 epochs (Fig. 3 *A*). At this low N, even though release is almost perfectly regular and quantal noise has been almost completely eliminated, continuous rod voltage noise remains. In the absence of quantal noise, the physiological voltage noise, $\pm$0.2 mV, widens the Q_{count} distribution and contributes an SD of $\sim$0.4 Q to it (Appendix B of Schein and Ahmad (1)). As a result, even complete elimination of quantal noise would not be able to reduce the probability of false positives to 1 in 16,000 epochs for a lower $Q_{rate,dark}$ like 92 or 91 Q s^{-1}.

In summary, for a lower $Q_{rate,dark}$, regularity as expressed by Erlang order r must be higher, the requisite narrowing N must be lower, and efficiency is higher. For a higher $Q_{rate,dark}$, regularity must be lower, the requisite narrowing N must be higher, and efficiency is lower.

Fig. 3, *A* and *B*, shows narrowing N and efficiency, both as functions of $Q_{rate,dark}$. As shown in Fig. 3 *C*, we can also graph efficiency as a function of N: efficiency rises as N falls; that is, efficiency rises as Erlang order r rises.

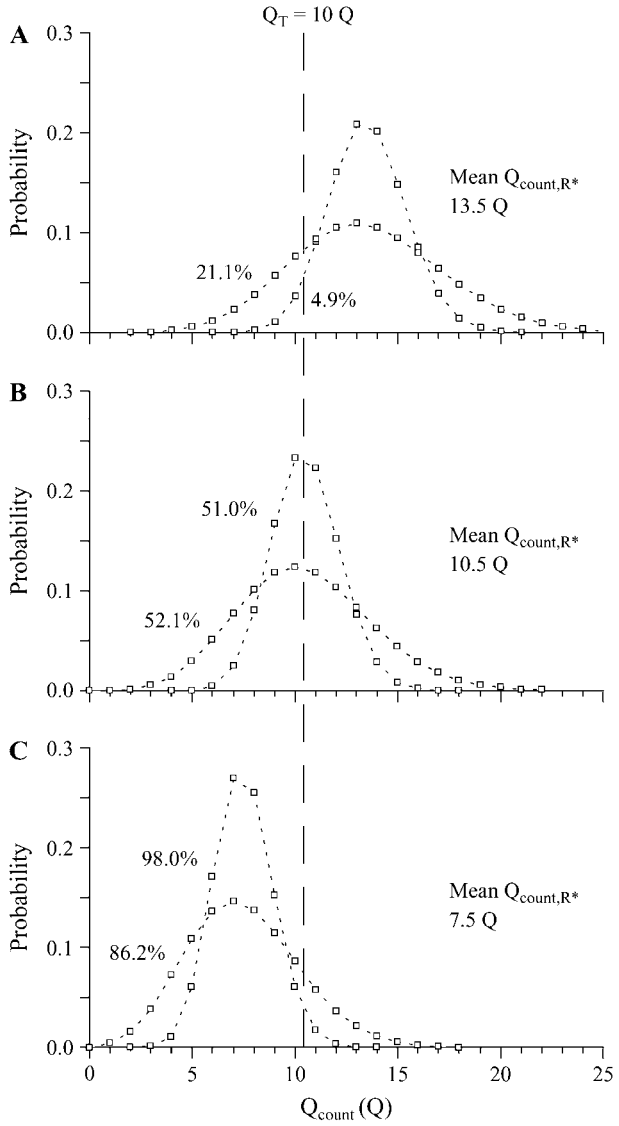

FIGURE 4 Narrower distribution (lower N) has lower efficiency if median $Q_{count} < Q_T$ or higher efficiency if median $Q_{count} > Q_T$. Here, Q_T is set to 10 Q. Efficiency is the sum of the probabilities for values of $Q_{count,R*} \leq Q_T$, that is, to the left of the dashed vertical line. Each part contains two distributions, the broader one with $N = 1$, the narrower with $N = 0.5$, and the symbols (□) in both are light because both represent $Q_{count,R*}$. (*A*) With mean and median $Q_{count,R*} > Q_T$, the narrower distribution has the lower efficiency. (*B*) With a mean and median $Q_{count,R*} \approx Q_T$, the width of the distribution has little effect on efficiency. (*C*) With a mean and median $Q_{count,R*} < Q_T$, the narrower distribution has the higher efficiency.

The same story holds with different Q_T and different ranges of $Q_{rate,dark}$

Like Fig. 3, Fig. 5 shows the relationships among $Q_{rate,dark}$, narrowing N, and efficiency, but it does so for a many values of Q_T, ranging from 0 Q to 15 Q.

Fig. 5 *B* shows that high efficiency is possible with very low $Q_{rates,dark}$. Indeed, an efficiency of 64% can be achieved with a $Q_{rate,dark}$ of 12 Q s^{-1} if Q_T is 0 Q; however, the

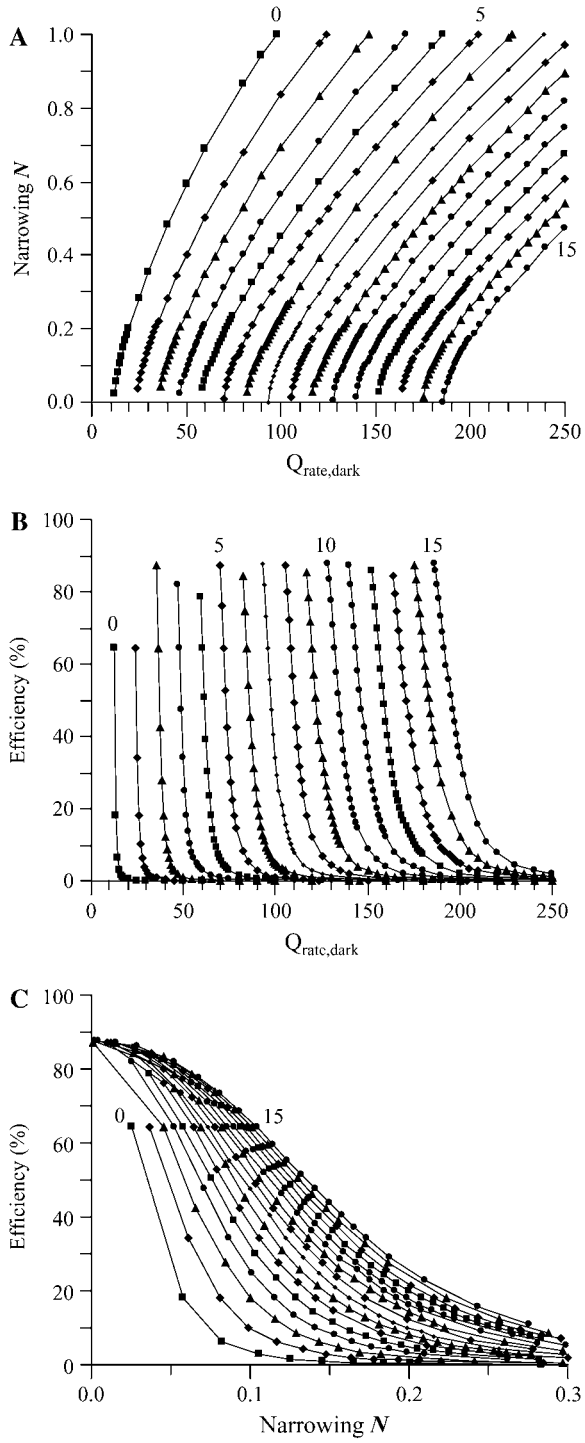

FIGURE 5 Relationships among $Q_{rate,dark}$, narrowing N, and efficiency of transmission for quantal thresholds Q_T from 0 Q to 15 Q. (*A*) Narrowing N as a function of $Q_{rate,dark}$. (*B*) Efficiency as a function of $Q_{rate,dark}$. (*C*) Efficiency as a function of narrowing N. These data make the same ''standard assumptions'' listed in the legend of Fig. 2 for probability of false positives, duration of counting window, and decrement. Because $Q_{rate,dark}$ is not restricted to integers, the points in each family (marked with the value of Q_T) are connected by a solid curve. The data for $Q_T = 7$ Q is the same as in Fig. 3.

narrowing N must be set very close to zero, 0.026 (Fig. 5 *A*). To achieve such a low N, release would have to be almost perfectly regular. Fig. 6, on the left, shows the $Q_{count,dark}$ and $Q_{count,light}$ distributions that would give this remarkable result.

As was shown by Fig. 3 *B*, for a Q_T of 7 Q and a high $Q_{rate,dark}$, 120 Q s^{-1}, efficiency is very low indeed. However, Fig. 5 *B* shows that a high $Q_{rate,dark}$ like 120 Q s^{-1} can produce high efficiency if Q_T is set to an appropriately high value (like 9 Q). Fig. 6, on the right, shows the $Q_{count,dark}$ and $Q_{count,light}$ distributions that would give this result.

Many of the same efficiency values show up in many of the Q_T curves in Fig. 5 *B*. For example, an efficiency of 34% may be achieved for a $Q_{rate,dark}$ of 50 Q s^{-1} with $Q_T = 3$ Q and for a $Q_{rate,dark}$ of 100 Q s^{-1} with $Q_T = 7$ Q as well. The release process must be more regular in the former than in the latter case, $N = 0.087$ versus $N = 0.123$ (Fig. 5 *A*).

Indeed, the different Q_T families of points in each part of Fig. 5, *A* and *B*, appear to be simple transformations of each other. Beginning with Fig. 5 *B*, any particular efficiency can be obtained with many combinations of $Q_{rate,dark}$ and Q_T. As in the above example, an efficiency of 34% can be obtained for a $Q_{rate,dark}$ of 100 Q s^{-1} with $Q_T = 7$ Q and a $Q_{rate,dark}$ of 50 Q s^{-1} with $Q_T = 3$ Q. The ratio of $Q_{rates,dark}$ (100/50) is equal to the ratio of the $Q_T + 1$ values, in this case, (7 + 1)/(3 + 1). Thus,

$$\frac{Q_{rate,dark2}}{Q_{rate,dark1}} = \frac{Q_{T2} + 1}{Q_{T1} + 1}. \quad (1)$$

(Had we defined Q_T as giving a positive event when $Q_{count} < Q_T$ instead of when $Q_{count} \leq Q_T$, the Q_T in these two cases would have been 8 Q and 4 Q, and the ratio in Eq. 1 would have been just Q_{T2}/Q_{T1}.) Correctly following this equation, an efficiency of 34% may be obtained for a $Q_{rate,dark}$ of 200 Q s^{-1} if Q_T is set to 15 Q. Note that $Q_{rate,dark}$ is not restricted to integer rates; for example, this efficiency may also be obtained for a Q_T of 6 Q if $Q_{rate,dark}$ is 87.5 Q s^{-1}.

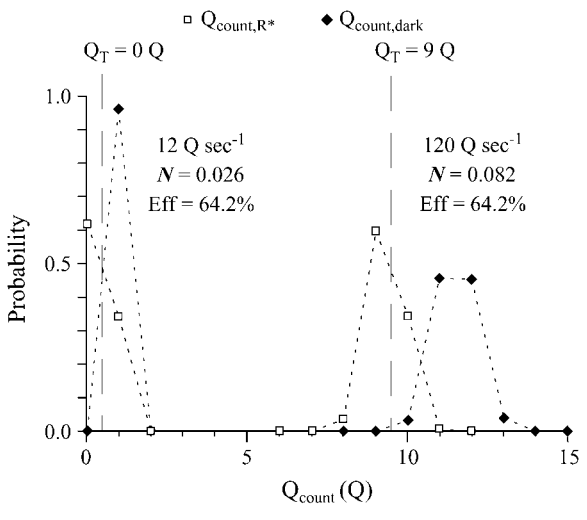

FIGURE 6 High efficiency can be achieved with a wide range of $Q_{rates,dark}$. These two examples, with a $Q_{rate,dark}$ of 12 Q s^{-1} on the left and a $Q_{rate,dark}$ of 120 Q s^{-1} on the right, have the same efficiency (64.2%).

In Fig. 5 *A*, for the same combinations of $Q_{rate,dark}$ and Q_T (e.g., 100 Q s^{-1} and 7 Q vs. 200 Q s^{-1} and 15 Q) that give an efficiency of 34%, N is related by the square root of the ratio of the $Q_{rates,dark}$. Thus, for 100 Q s^{-1} on the $Q_T = 7$ Q curve, $N = 0.123$. For 200 Q s^{-1} on the $Q_T = 15$ Q curve, $N = 0.173$, increased by the factor $\sqrt{200/100} = \sqrt{2}$. Thus,

$$\frac{N_2}{N_1} = \sqrt{\frac{Q_{rate,dark2}}{Q_{rate,dark1}}}. \quad (2)$$

Similarly, for 50 Q s^{-1} on the $Q_T = 3$ Q curve, $N = 0.087$, reduced from 0.123 by $\sqrt{2}$.

Therefore, in Fig. 5 *C*, to obtain a particular efficiency like 34%, as Q_T increases from 3 Q to 7 Q, $Q_{rate,dark}$ must increase by a factor of [(7 + 1)/(3 + 1)] = 2, and N must increase by the square root of this factor, $\sqrt{2}$. The three parameters $Q_{rate,dark}$, Q_T, and N, are thus tightly linked. Indeed, given one set of Q_T curves, like the N versus $Q_{rate,dark}$ curve for $Q_T = 7$ Q (Fig. 3 *A*) and the efficiency versus $Q_{rate,dark}$ curve for $Q_T = 7$ Q (Fig. 3 *B*), we can by use of Eqs. 1 and 2 produce all of the Q_T families of points in Fig. 5, *A–C*.

Efficiency depends on a single parameter, CV_{dark}

The relationships in Eqs. 1 and 2 suggest that efficiency could be plotted as a function of a single parameter, $N/\sqrt{Q_{rate,dark}}$, and then all of the Q_T families of points in Fig. 5, *A* and *B*, would collapse into one curve. However, because efficiency is determined by a comparison between $Q_{count,dark}$ and $Q_{count,R*}$ distributions, it is useful to transform first the $Q_{rates,dark}$ into mean $Q_{counts,dark}$ by multiplying the former by 0.1 s; hence,

$$\frac{N}{\sqrt{0.1 \times Q_{rate,dark}}} = \frac{N}{\sqrt{\text{mean}\, Q_{count,dark}}} = CV_{dark}, \quad (3)$$

with a discussion of CV_{dark} to follow.

The term CV_{dark} has physical meaning. Coefficient of variation (CV), a measure of the relative width of a distribution, equals the SD of a distribution divided by the mean. For a count distribution generated by a Poisson process, the SD equals the $\sqrt{\text{mean count}}$, and $CV_{Poisson}$ equals $\sqrt{\text{mean count}}/\text{mean count} = 1/\sqrt{\text{mean count}}$. Thus, Eq. 3 could be rewritten as

$$CV_{dark} = N \times CV_{Poisson}. \quad (4)$$

For a count distribution generated by an Erlang or gamma process, the SD and thus the CV is reduced approximately by the factor N compared to the count distribution generated by a Poisson process, as described in Methods. Therefore, the term CV_{dark} in Eqs. 3 and 4 is approximately equal to the coefficient of variation of a $Q_{count,dark}$ distribution generated by an Erlang or gamma process, hence the name CV_{dark}.

Indeed, as shown by Fig. 7 *A*, when efficiency is plotted as a function of CV_{dark}, several—a selection—of the different Q_T families of efficiency from Fig. 5 collapse onto one curve, with higher efficiency for lower CV_{dark}. In Fig. 7 *B*, the selected families are displaced to make each family visible. It is worth noting that all of the Q_T families of efficiencies would lie on just one curve when graphed against any function of CV_{dark} on the abscissa, including, for example, its reciprocal.

The specific curve in Fig. 7 *A* obtains only for a specific set of three other parameters that we fix in this article. First, the requisite narrowing N of the $Q_{count,dark}$ distribution depends on the probability of false positives due to quantal noise and rod voltage noise: We assumed 1 in 16,000 epochs. Second, the mean $Q_{count,dark}$ is close to the product of $Q_{rate,dark}$ and the counting window: We assumed 0.1 s for the counting window. (Actually, the mean $Q_{count,dark}$ is slightly less than this product, called M, as described in Methods.) Third, the efficiency is the fraction of the $Q_{count,R*}$ distribution that is $\leq Q_T$, and the mean of the $Q_{count,R*}$ distribution depends on the decrement in Q_{rate} in response to production of one R*: We assumed a decrement of 18.1%, produced by a 1 mV hyperpolarization and an *e*-fold reduction in Q_{rate} for 5 mV. Therefore, throughout this article, we fixed 1), the probability of a false positive; 2), the duration of the counting window; and 3), the decrement in Q_{rate}.

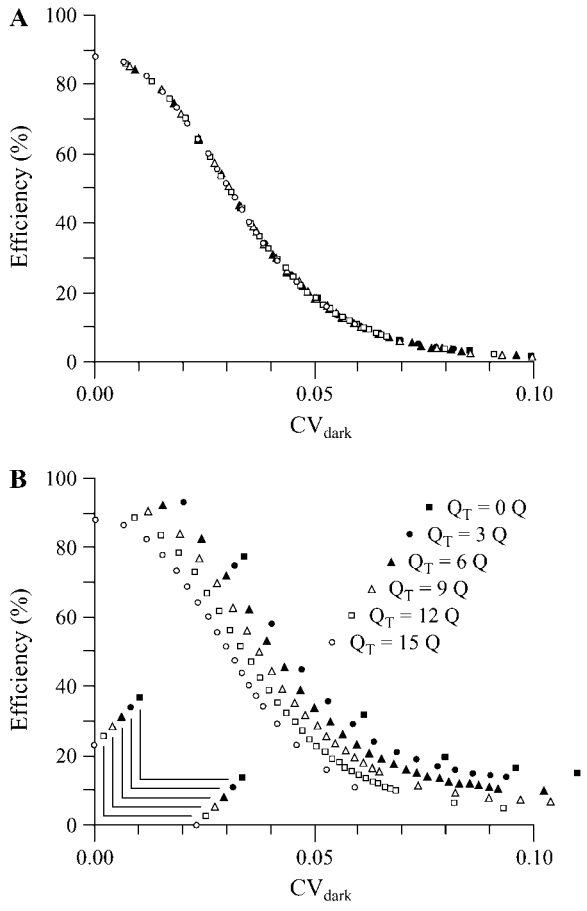

FIGURE 7 Efficiency is a function of a single parameter, CV_{dark}. (*A*) The efficiencies from a selection of the Q_T families collapse into one curve. (*B*) To be able to see each Q_T family of efficiencies, the selected Q_T families are shown displaced one from another along both abscissa and ordinate. Because $Q_{rate,dark}$ is not restricted to integers, the points in each family could be connected by a solid curve.

Measurement of efficiency reveals CV_{dark} but not $Q_{rate,dark}$ or N

As shown by any horizontal line in Fig. 5, *B* or *C*, many combinations of parameters can produce a given efficiency. These isoefficiency combinations yield the same CV_{dark} (Fig. 7 *A*). As a specific example, the combinations of N and $Q_{rate,dark}$ that yield 50% efficiency are shown in Fig. 8 for Q_T ranging from 0 Q to 15 Q. For $Q_T = 0$ Q, the Q_{rate} would be 12.208 Q s^{-1}. (In that case, the $Q_{count,dark}$ would be 0 Q in 1 of 16,000 epochs and 1 Q in 15,599 of 16,000 epochs. In addition, the $Q_{count,R*}$ would be 0 Q in exactly half of the epochs and 1 Q in the other half, hence 50% efficiency.) This $Q_{rate,dark}$ is slightly greater than the rate (12 Q s^{-1}) that gave an efficiency of 64% in Fig. 6. To achieve the same CV_{dark} (0.0307) for all of the points in Fig. 8 (and to maintain the ''standard'' probability of one false positive per 16,000 epochs), N increases as the square root of $Q_{rate,dark}$. And, as Q_T steps by increments of 1 Q, $Q_{rate,dark}$ steps by increments of 12.208 Q s^{-1}. Therefore, even with a fixed counting window, a fixed decrement, and a fixed probability of a false positive, measurement of efficiency reveals CV_{dark} but not the individual values of $Q_{rate,dark}$ or N.

Efficiency improves for higher $Q_{rate,dark}$ if Q_T is increased

In our previous article (1), we reported that efficiency rose from 1% to 5% to 12% to 32% as $Q_{rate,dark}$ doubled from

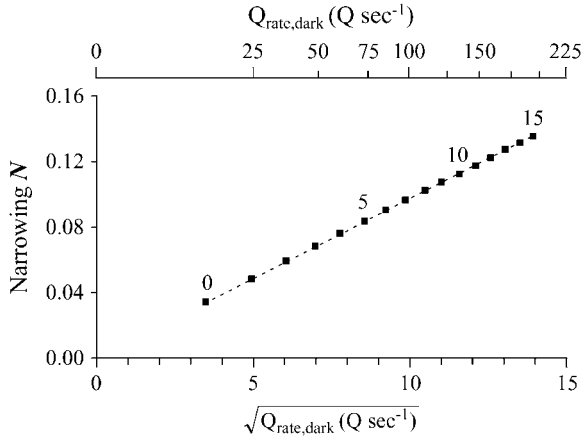

FIGURE 8 To obtain a particular efficiency, like 50%, N is directly proportional to $\sqrt{Q_{rate,dark}}$. These points are fit by the equation $N = 0.0097 \times \sqrt{Q_{rate,dark}}$.

50 to 100 to 200 to 400 Q s^{-1}. That finding can now be understood in the broader context of the current findings, as shown in Fig. 9: As rates double from 50 through 400 Q s^{-1}, with all of the Q_{count} distributions having nearly the same $N \approx 0.24$, overlap between $Q_{count,dark}$ and Q_{count,R^*} distributions falls. Efficiency would crash if Q_T were fixed, but it rises if Q_T is able to rise to take advantage of the shift of the Q_{count} distributions to higher values.

By contrast, in this article, a small increase in $Q_{rate,dark}$ (e.g., from 100 Q s^{-1} to 101 Q s^{-1}) is not enough to permit an upward shift of Q_T (from 6 Q to 7 Q, for example). Q_T is thus necessarily fixed. As shown in Fig. 2 for fixed Q_T, as $Q_{rate,dark}$ rises Q_{rate,R^*} rises proportionately, the Q_{count,R^*} distribution moves rightward, a smaller percentage of the Q_{count,R^*} distribution is $\leq Q_T$, and efficiency falls.

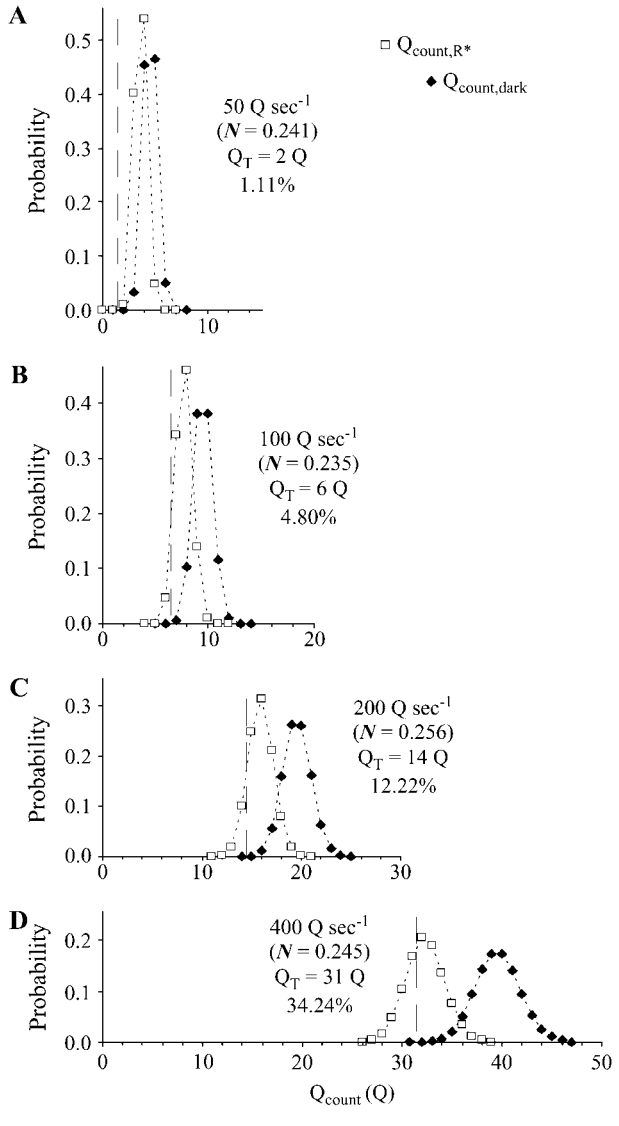

FIGURE 9 For similar N, efficiency rises as Q_{rate} rises if Q_T rises suitably as well. (*A*) $Q_{rate,dark} = 50$ Q s^{-1}. (*B*) $Q_{rate,dark} = 100$ Q s^{-1}. (*C*) $Q_{rate,dark} = 200$ Q s^{-1}. (*D*) $Q_{rate,dark} = 400$ Q s^{-1}.

DISCUSSION

We investigated how the efficiency of transmission by a rod photoreceptor of a single-photon event changes for a small change in the quantal release rate in the dark ($Q_{rate,dark}$) and a proportionately small change in the quantal release rate for one isomerization of rhodopsin (Q_{rate,R^*}). This investigation produced several new findings. First, as shown in Fig. 3, efficiency falls—and falls steeply—as $Q_{rate,dark}$ rises. As shown in Fig. 2, it falls primarily because the distribution of quantal count for one isomerization of rhodopsin (Q_{count,R^*}) moves rightward, and a smaller percentage of this distribution is less than or equal to a quantal-count threshold (Q_T).

Second, as shown in Fig. 5, the curves showing efficiency as a function of $Q_{rate,dark}$ are different for each Q_T but are systematically related, as given by Eqs. 1 and 2. For that reason, as shown in Fig. 7, all of these curves collapse into one when plotted against CV_{dark}, a parameter that combines degree of regularity (Erlang order r) and $Q_{count,dark}$. Third, because the key parameter CV_{dark} involves order r as well as $Q_{rate,dark}$, measurement of efficiency (e.g., 50%) by itself cannot reveal the $Q_{rate,dark}$. Fourth, for that reason, as shown in Fig. 6, high efficiency could be achieved even with a very low $Q_{rate,dark}$ if order r is great enough.

These findings hold irrespective of whether the rod bipolar dendrite actually counts in whole numbers (quanta) or transforms that count into a continuous variable. Consideration of the consequences and opportunities presented by such a transformation leads to several additional findings, which follow.

The biochemically realized values of Q_{count} and Q_T in a bipolar dendrite may be noninteger

The cascade that couples mGluR6 activation to closure of cation-selective channels on the rod bipolar dendrite remains a puzzle (28–31). Nonetheless, the postsynaptic response to a quantum of glutamate, as measured by the change in concentration or activity of these coupling elements, must have a time course. As a result, a quantum released late in the 0.1 s ''counting window'' or before—but close to—the start of the 0.1 s ''counting window'' would have partial effect. Moreover, the effects of quanta released at different times in the counting window may differ. These partially or differently weighted effects yield the equivalent of noninteger numbers of quanta within the counting window. Thus, the biochemical realizations of $Q_{count,dark}$ and $Q_{count,light}$ in a bipolar dendrite may assume noninteger values.

In the bipolar dendrite, Q_T is also realized biochemically, by the concentration of coupling elements like second messengers or the level of activity of enzymes. We can call the value of such a quantity the ''biochemical Q_T''. Like the biochemical Q_{counts}, the biochemical Q_T may take noninteger values. For example, according to the threshold mechanism modeled by van Rossum and Smith (5), ''messengerase'' enzyme activity in the dark is in excess of what is needed to

hold the concentration of intracellular messenger at zero. Because it is in excess, messengerase activity must fall to some threshold level before the concentration of messenger is able to rise above zero and open channels. Thus, Q_{rate} must fall below some (threshold) rate to drop Q_{count} low enough (to some threshold count) to permit messengerase to fall to some low (threshold) activity to allow the concentration of messenger to rise above zero and open messenger-gated channels. None of these biochemical threshold parameters are quantal in nature.

The bipolar dendrite could regulate Q_T and Q_{count}

Many parameters enter into the mathematics of the rod bipolar dendrite's decision between a photon and darkness: $Q_{rate,dark}$, the counting window, Erlang order r, the mean and the SD of the $Q_{count,dark}$ distribution, the probability of a false positive due to quantal noise and rod voltage noise, Q_T, the decrement in $Q_{rate,dark}$ due to production of one R* (yielding Q_{rate,R^*}), and the mean and the SD of the Q_{count,R^*} distribution. However, $Q_{rate,dark}$ and the decrement (and therefore Q_{rate,R^*}) and order r are set presynaptically. In addition, within the rod bipolar dendrite some of these parameters are likely to be fixed, like the counting window. Other parameters are tightly linked: the mean and SD of the $Q_{count,dark}$ distribution are determined by $Q_{rate,dark}$, the counting window, and order r. The probability of a false positive is determined by Q_T and the mean and SD of the $Q_{count,dark}$ distribution. The mean and SD of the Q_{count,R^*} distribution are determined by the mean $Q_{count,dark}$ and order r. By this logic, only one parameter remains for the rod bipolar cell to regulate, the biochemical Q_T.

However, Q_{counts} are transformed into biochemical Q_{counts} in the rod bipolar dendrite by the cascade that couples activation of the mGluR6 receptor (32–43). Therefore, the biochemical $Q_{count,dark}$ and Q_{count,R^*} are proportional to the strength of this coupling and should also be subject to regulation by the bipolar dendrite. Indeed, most of the effects on the bipolar response of variation in intracellular [Ca^{2+}] (29,44–49), cyclic nucleotides (29,50), and the activity of different enzymes that modulate the cascade (31,46,47,49–51) may therefore be described in terms of change in the biochemical Q_{counts}.

Maintaining the relationship between the biochemical Q_T and Q_{count,R^*} would stabilize efficiency

For any fixed Q_T, if $Q_{rate,dark}$ drifts upward, efficiency falls steeply (Figs. 3 *B* and 5 *B*). For example, starting with conditions for 50% efficiency (e.g., $Q_{rate,dark} = 97.66$ Q s^{-1}, $Q_T = 7$ Q, and $N = 0.0958$), if $Q_{rate,dark}$ rose by only 5% (to 102.54 Q s^{-1}, with $N = 0.1486$), efficiency would drop to 22.7% (Fig. 3 *B*). Or, if N remained at 0.0958, efficiency would drop from 50% to 17.6%. Indeed, starting from any combination of $Q_{rate,dark}$ and N that yields an efficiency of 50%, an increase of $Q_{rate,dark}$ by 5% (with unchanging N) would drop efficiency to 17.6% (Fig. 7).

$Q_{rate,dark}$ depends on membrane potential in the synaptic terminal of the rod and is likely to drift somewhat, perhaps even more than ±5%. In the face of such drift, how could the efficiency of the transmission from rod to rod bipolar dendrite be maintained within small limits?

A likely mechanism follows from the observation that the primary determinant of efficiency is the relative position of mean Q_{count,R^*} and Q_T (Fig. 2). In Results, Q_T is quantal, that is, restricted to values like 7 Q or 6 Q. However, as described above, the biochemical Q_T in a bipolar cell dendrite is a continuous value that could, for example, rise to a mean of 7.35 Q, 5% higher than 7 Q in response to a rise in mean Q_{count,R^*} by 5%. Thus, if the biochemical Q_T rose or fell with Q_{rate,R^*} (and $Q_{rate,dark}$), efficiency would be stable. Alternatively, if Q_T held steady but the coupling strength of the cascade was reduced by 5%, countering the 5% rise in Q_{rate,R^*} and holding the biochemical Q_{rate,R^*}, efficiency would be stable.

In an even better scenario, Q_T and median Q_{rate,R^*} would be equal because efficiency, which would be 50%, would be immune to change in N, as shown by Fig. 4 *B*. Indeed, efficiency is close to this value: Field and Rieke (10) reported an efficiency of 25%, but our analysis of their data suggested 35–40% (1), and Taylor and Smith (52) and Berntson et al. (53) estimated 60%.

However, assuming that Q_T was equal to median Q_{rate,R^*}, variation in N would still affect the probability of a false positive due to quantal noise and rod voltage noise. Such an effect would be easily tolerated if the interval between these false positives (e.g., 1600 s) were much greater than the interval (~160 s) between spontaneous isomerizations of rhodopsin (11).

What conditions would produce 50% efficiency? As described in Methods, the biological $Q_{rate,dark}$ is likely to total ~100 Q s^{-1} for the two active zones associated with the two ribbon synaptic units in a mammalian rod (19). As detailed above and in Fig. 8, for a $Q_{rate,dark}$ of slightly less than 100 Q s^{-1}, 50% efficiency could be generated for a Q_T of 7 Q by an N of ~0.1 (Erlang order $r \approx 100$).

The regulation mechanism

If a rod bipolar cell has just responded, negative feedback could reduce its likelihood of responding again, that is, reduce the efficiency of transmission. As illustrated by Fig. 2, it could do so by reducing its biochemical Q_T or by increasing the mean of its biochemical Q_{count,R^*}. In terms of the threshold mechanism proposed by van Rossum and Smith (5) and described two sections above, reducing the biochemical Q_T could correspond to reducing the concentration of messenger by reducing its rate of production in the dark. Raising the biochemical Q_{count,R^*} (and $Q_{count,dark}$) could correspond to raising the activity of the messengerase enzyme.

Both mechanisms are employed to accomplish negative feedback in an olfactory receptor cell that (like the rod bipolar cell) depolarizes when stimulated (54). The cell depolarizes because odorant binding stimulates an adenylyl cyclase, which increases the concentration of cAMP, which opens cation channels that also flux Ca^{2+}. The feedback occurs when interaction of the higher intracellular concentration of Ca^{2+} with calmodulin both reduces the activity of an adenylyl cyclase (analogous to reducing Q_T) and increases the activity of a cAMP phosphodiesterase (analogous to raising Q_{count,R^*}).

Likewise, stimulation (by a photon) causes depolarization of a rod bipolar dendrite as a result of the opening of cation-selective channels (55,56) that can flux Ca^{2+} (45,48). Acting as negative feedback, the increased intracellular concentration of Ca^{2+} reduces sensitivity to light by two mechanisms, desensitization and ''use-dependent depression'' (29). The former has a time constant of ~1 s, whereas the latter has a time constant of ~10 min. Ca^{2+} entry and these periods of reduced sensitivity depend on R* events, so they are ''event-based''.

Conversely, when the dendrite has failed to respond to an R* for a ''long time'', the reduced intracellular concentration of Ca^{2+} would increase the dendrite's likelihood of responding, that is, increase the efficiency of transmission. How long is a ''long time''? Under starlight conditions, photon capture by an individual rod is rare, perhaps once in several thousand epochs (8,57); in complete darkness, no photons are captured at all. Spontaneous isomerization of rhodopsin is more frequent, approximately once every ~160 s in each rod (11). If transmission efficiency were 50%, each rod bipolar dendrite would experience a positive event on average once every ~320 s, ~5 min, within the time constant of use-dependent depression (48,49). Thus, spontaneous isomerization of rhodopsin could play a beneficial role, providing the signal that may be used to stabilize efficiency of transmission at the synapse between a rod and a rod bipolar dendrite.

We thank Karen Migdale for discussions that triggered this work and Robert Smith for generously and consistently providing insightful discussion.

REFERENCES

1. Schein, S., and K. M. Ahmad. 2005. A clockwork hypothesis: synaptic release by rod photoreceptors must be regular. *Biophys. J.* 89:3931–3949.
2. Sterling, P., and G. Matthews. 2005. Structure and function of ribbon synapses. *Trends Neurosci.* 28:20–29.
3. Rieke, F., and E. A. Schwartz. 1996. Asynchronous transmitter release: control of exocytosis and endocytosis at the salamander rod synapse. *J. Physiol. (Lond.).* 493:1–8.
4. Rao-Mirotznik, R., G. Buchsbaum, and P. Sterling. 1998. Transmitter concentration at a three-dimensional synapse. *J. Neurophysiol.* 80: 3163–3172.
5. van Rossum, M. C., and R. G. Smith. 1998. Noise removal at the rod synapse of mammalian retina. *Vis. Neurosci.* 15:809–821.
6. Choi, S. Y., B. Borghuis, R. Rea, E. S. Levitan, P. Sterling, and R. H. Kramer. 2005. Encoding light intensity by the cone photoreceptor synapse. *Neuron.* 48:555–562.
7. Hood, D. C., and M. A. Finkelstein. 1986. Sensitivity to light. *In* Handbook of Perception and Human Performance, Vol. 1: Sensory Processes and Perception. K. R. Boff, L. Kaufman, and J. P. Thomas, editors. John Wiley & Sons, New York. 5.1–5.66.
8. Walraven, J., C. Enroth-Cugell, D. C. Hood, D. I. A. MacLeod, and J. L. Schnapf. 1990. The control of visual sensitivity: Receptoral and postreceptoral processes. *In* The Neurophysiological Foundations of Visual Perception. L. Spillman, and J. Werner, editors. Academic Press, San Diego, CA. 53–101.
9. Robson, J. G., and L. J. Frishman. 1999. Dissecting the dark-adapted electroretinogram. *Doc. Ophthalmol.* 95:187–215.
10. Field, G. D., and F. Rieke. 2002. Nonlinear signal transfer from mouse rods to bipolar cells and implications for visual sensitivity. *Neuron.* 34:773–785.
11. Baylor, D. A., B. J. Nunn, and J. L. Schnapf. 1984. The photocurrent, noise and spectral sensitivity of rods of the monkey *Macaca fascicularis*. *J. Physiol. (Lond.).* 357:575–607.
12. Schneeweis, D. M., and J. L. Schnapf. 1995. Photovoltage of rods and cones in the macaque retina. *Science.* 268:1053–1056.
13. Sampath, A. P., and R. Rieke. 2004. Selective transmission of single photon responses by saturation at the rod-to-rod bipolar synapse. *Neuron.* 41:431–443.
14. Field, G. D., A. P. Sampath, and R. Rieke. 2005. Retinal processing near absolute threshold: from behavior to mechanism. *In* Annual Review of Physiology, Vol. 67. J. F. Hoffman, editor. Annual Reviews, Palo Alto, CA. 491–514.
15. Thoreson, W. B., R. Katalin, E. Townes-Anderson, and R. Heidelberger. 2004. A highly Ca^{2+}-sensitive pool of vesicles contributes to linearity at the rod photoreceptor ribbon synapse. *Neuron.* 42:595–605.
16. Collins, M. O., Y. Lu, M. P. Coba, H. Husi, I. Campuzano, W. P. Blackstock, J. S. Choudhary, and S. G. N. Grant. 2005. Proteomic analysis of in vivo phosphorylated synaptic proteins. *J. Biol. Chem.* 280:5972–5982.
17. de Ruyter van Steveninck, R. R., G. D. Lewen, S. P. Strong, R. Koberle, and W. Bialek. 1997. Reproducibility and variability in neural spike trains. *Science.* 275:1805–1808.
18. Berry, M. J., and M. Meister. 1998. Refractoriness and neural precision. *J. Neurosci.* 18:2200–2211.
19. Migdale, K., S. Herr, K. Klug, K. Ahmad, K. Linberg, P. Sterling, and S. Schein. 2003. Two ribbon synaptic units in rod photoreceptors of macaque, human, and cat. *J. Comp. Neurol.* 455:100–112.
20. Townes-Anderson, E., P. R. MacLeish, and E. Raviola. 1985. Rod cells dissociated from mature salamander retina: Ultrastructure and uptake of horseradish peroxidase. *J. Cell Biol.* 100:175–188.
21. Barlow, H. B. 1956. Retinal noise and absolute threshold. *J. Opt. Soc. Am.* 8:634–639.
22. Donner, K. 1992. Noise and the absolute thresholds of cone and rod vision. *Vision Res.* 32:853–866.
23. Rodieck, R. W. 1998. The First Steps in Seeing. Sinauer, Sunderland, MA.
24. Bader, C. R., D. Bertrand, and E. A. Schwartz. 1982. Voltage-activated and calcium-activated currents studied in solitary rod inner segments from the salamander retina. *J. Physiol. (Lond.).* 331: 253–284.
25. Corey, D. P., J. M. Dubinsky, and E. A. Schwartz. 1984. The calcium current in inner segments of rods from the salamander (*Ambystoma tigrinum*) retina. *J. Physiol. (Lond.).* 354:557–575.
26. Taylor, W. R., and C. Morgans. 1998. Localization and properties of voltage-gated calcium channels in cone photoreceptors of *Tupaia belangeri*. *Vis. Neurosci.* 15:541–552.
27. Schneeweis, D. M., and D. L. Schnapf. 2000. Noise and light adaptation in rods of the macaque monkey. *Vis. Neurosci.* 17:659–666.
28. Nawy, S. 1999. The metabotropic receptor mGluR6 may signal through G(o), but not phosphodiesterase, in retinal bipolar cells. *J. Neurosci.* 19:2938–2944.

29. Nawy, S. 2004. Desensitization of the mGluR6 transduction current in tiger salamander On bipolar cells. *J. Physiol. (Lond.).* 558:137–146.

30. Dhingra, A., M. Jiang, T. L. Wang, A. Lyubarsky, A. Savchenko, T. Bar-Yehuda, P. Sterling, L. Birnbaumer, and N. Vardi. 2002. Light response of retinal ON bipolar cells requires a specific splice variant of Gα(o). *J. Neurosci.* 22:4878–4884.

31. Dhingra, A., E. Faurobert, N. Dascal, P. Sterling, and N. Vardi. 2004. A retinal-specific regulator of G-protein signaling interacts with $G\alpha_o$ and accelerates an expressed metabotropic glutamate receptor 6 cascade. *J. Neurosci.* 24:5684–5693.

32. Slaughter, M. M., and R. F. Miller. 1981. 2-Amino-4-phosphonobutyric acid: a new pharmacological tool for retina research. *Science.* 211: 182–185.

33. Nakajima, Y., H. Iwakabe, C. Akazawa, H. Nawa, R. Shigemoto, N. Mizuno, and S. Nakanishi. 1993. Molecular characterization of a novel retinal metabotropic glutamate receptor mGluR6 with a high agonist selectivity for L-2-amino-4-phosphonobutyrate. *J. Biol. Chem.* 268:11868–11873.

34. Nomura, A., R. Shigemoto, Y. Nakamura, N. Okamoto, N. Mizuno, and S. Nakanishi. 1994. Developmentally-regulated postsynaptic localization of a metabotropic glutamate-receptor in rat rod bipolar cells. *Cell.* 77:361–369.

35. Pin, J. P., and R. Duvoisin. 1995. The metabotropic glutamate receptors: structure and functions. *Neuropharmacology.* 34:1–26.

36. Vardi, N., and K. Morigiwa. 1997. ON cone bipolar cells in rat express the metabotropic receptor mGluR6. *Vis. Neurosci.* 14:789–794.

37. Nelson, R. 1973. A comparison of electrical properties of neurons in *Necturus* retina. *J. Neurophysiol.* 36:519–535.

38. Toyoda, J. 1973. Membrane resistance changes underlying the bipolar cell response in the carp retina. *Vision Res.* 13:283–294.

39. Nawy, S., and C. E. Jahr. 1990. Suppression by glutamate of cGMP-activated conductance in retinal bipolar cells. *Nature.* 346:269–271.

40. Shiells, R. A., and G. Falk. 1990. Glutamate receptors of rod bipolar cells are linked to a cyclic GMP cascade via a G-protein. *Proc. R. Soc. Lond. B Biol. Sci.* 242:91–94.

41. Shiells, R. A., and G. Falk. 1992. Properties of the cGMP-activated channel of retinal on-bipolar cells. *Proc. R. Soc. Lond. B Biol. Sci.* 247: 21–25.

42. de la Villa, P., T. Kurahashi, and A. Kaneko. 1995. L-glutamate-induced responses and cGMP-activated channels in three subtypes of retinal bipolar cells dissociated from the cat. *J. Neurosci.* 15:3571–3582.

43. Euler, T., H. Schneider, and H. Wässle. 1996. Glutamate responses of bipolar cells in a slice preparation of the rat retina. *J. Neurosci.* 16: 2934–2944.

44. Walters, R. J., R. H. Kramer, and S. Nawy. 1998. Regulation of cGMP-dependent current in On bipolar cells by calcium/calmodulin-dependent kinase. *Vis. Neurosci.* 15:257–261.

45. Shiells, R. A., and G. Falk. 1999. A rise in intracellular Ca^{2+} underlies light adaptation in dogfish retinal ''on'' bipolar cells. *J. Physiol. (Lond.).* 514:343–350.

46. Shiells, R.A., and G. Falk. 2000. Activation of Ca^{2+}-calmodulin kinase II induces desensitization by background light in dogfish retinal ''on'' bipolar cells. *J. Physiol. (Lond.).* 528:327–338.

47. Shiells, R.A., and G. Falk. 2001. Rectification of cGMP-activated channels induced by phosphorylation in dogfish retinal ''on'' bipolar cells. *J. Physiol. (Lond.).* 535:697–702.

48. Nawy, S. 2000. Regulation of the on bipolar cell mGluR6 pathway by Ca^{2+}. *J. Neurosci.* 20:4471–4479.

49. Snellman, J., and S. Nawy. 2002. Regulation of the retinal bipolar cell mGluR6 pathway by calcineurin. *J. Neurophysiol.* 88:1088–1096.

50. Shiells, R.A., and G. Falk. 2002. Potentiation of ''on'' bipolar cell flash responses by dim background light and cGMP in dogfish retinal slices. *J. Physiol. (Lond.).* 542:211–220.

51. Snellman, J., and S. Nawy. 2004. cGMP-dependent kinase regulates response sensitivity of the mouse on bipolar cell. *J. Neurosci.* 24:6621–6628.

52. Taylor, W. R., and R. G. Smith. 2004. Transmission of scotopic signals from the rod to rod-bipolar cell in the mammalian retina. *Vision Res.* 44:3269–3276.

53. Berntson, A., R. G. Smith, and W. R. Taylor. 2004. Transmission of single photon signals through a binary synapse in the mammalian retina. *Vis. Neurosci.* 21:693–702.

54. Fain, G. 2003. Sensory Transduction. Sinauer, Sunderland, MA. 173, 180.

55. Shiells, R. A., G. Falk, and S. Naghshineh. 1981. Action of glutamate and aspartate analogues on rod horizontal and bipolar cells. *Nature.* 294:592–594.

56. Nawy, S., and D. R. Copenhagen. 1987. Multiple classes of glutamate receptor on depolarizing bipolar cells in retina. *Nature.* 325:56–58.

57. Sampath, A., K. Strissel, R. Elias, V. Arshavsky, J. McGinnis, J. Chen, S. Kawamura, R. Rieke, and J. Hurley. 2005. Recoverin improves rod-mediated vision by enhancing signal transmission in the mouse retina. *Neuron.* 46:413–420.